

# Evaluation of low-dose CT supervised learning algorithms with transformer-based model observer

Yongyi Shi<sup>a</sup>, Ge Wang<sup>a</sup>, Xuanqin Mou<sup>b</sup>

<sup>a</sup>Biomedical Imaging Center, Rensselaer Polytechnic Institute, Troy, NY, USA

<sup>b</sup>Institute of Image Processing and Pattern Recognition, Xi'an Jiaotong University,  
Xi'an, Shaanxi, China

## ABSTRACT

A variety of supervise learning methods have been proposed for low-dose computed tomography (CT) sinogram domain denoising. Traditional measures of image quality have been employed to optimize and evaluate these methods, where mathematical model observers are widely advocated because it's designed to act as human surrogates in the task of lesion detectability for clinical diagnosis. However, the sinogram domain evaluation for the supervised learning methods remains lacking. Since the lesion in medical images is correspond to a narrow sine strip in sinogram domain, in this paper, we proposed a transformer-based efficient model observer to evaluate the sinogram domain supervise learning methods. The numerical results indicate that, we can well-approximate the Laguerre-Gauss channelized Hotelling observer (LG-CHO) models for a signal-known-exactly (SKE) and background-known-statistically (BKS) task by training a transformer-based model observer in sinogram domain. The proposed transformer-based model observer is then employed to assess three classic CNN-based sinogram domain denoising methods. The evaluation in these denoising methods may suggest future avenues for improving the effectiveness of sinogram domain supervised learning methods.

**Keywords:** model observer, transformer, computed tomography, sinogram domain denoising.

## INTRODUCTION

Low-dose computed tomography (CT) reconstruction is a hot topic in the CT field given that excessive X-ray radiation is harmful to human healthcare. It is crucial in low-dose CT reconstruction that the noise superimposed to CT data radiation due to limited quantum number of low-dose can be well suppressed. One way of the noise elimination is to preprocess sinogram data before reconstruction because of some advantages, such as the quantum noise in each detector element is independent to each other which benefits modeling the noise distribution and designing process algorithm, preprocessing sinogram data is highly efficient and the processed data is easily fed to succeeding reconstruction algorithms, and etc. More than a decade ago, Li et al. proposed a penalized likelihood method for quantum noise suppression for low-dose CT by investigating a model to determine the statistical property of projection data [1]. Wang et al. presented the penalized weighted least-squares approach to address projection domain denoising [2]. Manduca et al. [3] and Balda et al. [4] proposed two efficient approaches for projection domain denoising including bilateral filtering and structural adaptive filtering. Zhang et al. projection domain denoising method based on dictionary learning for low-dose CT image reconstruction [5]. Recently, convolutional neural network (CNN)-based supervised learning techniques have been proposed and widely investigated [6-9]. These methods are typically trained by minimizing the loss functions between the low-dose and full-dose sinogram, which usually achieve

high performance in terms of image quality metrics such as root mean square error (RMSE), peak signal-to-noise ratio (PSNR), structural similarity index metric (SSIM) [10] or feature similarity index metric (FSIM) [11]. However, it is well-known that such metrics may not consider the noise correlation which always present in CT images. To consider the strong noise correlation in CT images, the modulation transfer function (MTF) [12, 13] and the noise power spectrum (NPS) [14] are widely used to evaluate the image quality. However, Fourier based metrics assume linearity, and thus MTF and NPS would not be proper to evaluate the image quality for non-linear based image reconstruction such as CNN-based methods.

To assess image quality of CNN-based approaches in CT reconstruction, Bayesian ideal observer is a more appreciate choice when optimizing parameters of CNN for signal detection tasks (e.g., detection of a lesion), since lesion detectability is a common task in clinical diagnosis. Realization of a Bayesian ideal observer needs to know all statistical information of background and noise, which is not easy to acquire. Alternatively, Hotelling observer (HO) is a limited ideal observer model that employs the Hotelling discriminant to maximize the signal-to-noise ratio of the test statistic [9]. However, implementation of the HO requires the estimation and inversion of a covariance matrix that can be enormous [15]. Channelized Hotelling observer (CHO) approximates the HO utilizing efficient channels, which is more computationally tractable because of the reduction in data dimensionality [16]. A variety of CHOs are proposed through the use of different efficient channels. CHO with Laguerre-Gauss (LG) channels is applicable in scenarios where the signal is known exactly and rotationally symmetric [17, 18]. CHO with singular vectors (SV) requires the imaging system to be linear (or at least to be decomposed into linear and nonlinear processes) and that the system response is known [19]. CHO with partial least squares (PLS) channels overcome the challenges from the previous two approaches, that is, when the signal is not known exactly or not rotationally symmetric and when the imaging system response is not known [20]. Alternatively, CHO with Gabor channels facilitate the assessment of asymmetric text objects, do not require the imaging system response to known, and are not constrained to be rotationally symmetric [21]. However, all the aforementioned CHOs are still linear observers, which is suboptimal compared to the ideal observer (IO) performance for detection tasks in CT images.

Recent efforts have primarily focused on training model observes using deep learning, which provide an alternative solution to CT image quality assessment. Kopp et al proposed a CNN-based model observer in liver lesion detection task for X-ray CT [22]. Kim et al proposed a CNN-based model observer for signal-known-exactly (SKE) and background-known-statistically (BKS) detection tasks in breast CT images [23]. Gong et al proposed a CNN-based model observer to predict human performance in realistic CT tasks with varying patient anatomical background [24]. These CNN-based model observers are employed to optimize and evaluate the traditional reconstruction methods. Since the objective evaluation of image quality for the CNN-based low-dose CT reconstruction methods remains largely lacking, Li et al assessed deep neural network based denoising methods by use of CHOs [25]. Theoretically, an ideal observer achieves the upper bound of the image quality assessment on the detection task. In this regard, an ideal observer that evaluates a sinogram denoise algorithm should be designed to assess the performance of the signal detectability of the reconstructed image directly from the sinogram data. If this is so, the designed observer would not be influenced by variations of the used image reconstruction algorithm and therein parameter selection. Not only that, the variations may also include partial volume, beam hardening, directional noise artifacts, or motion artifacts introduced during reconstruction, and so on. Accomplishing such a task of developing a

sinogram based ideal observer involves numerous studies that bring all above mentioned influence factors in building the model. However, there is a primary question to be first answered, i.e., whether a sinogram based observer model could be well established? Though existing study suggested that it would be possible to detect a specific object from sinogram data [26], observer model design is required to accurately simulate human observer's performance that is more complicated. In this article, we report our preliminary study on developing sinogram based ideal observer model, i.e., we explore the property of sinogram connected the observer task and build a sinogram based observer model by mimicking a suboptimal observer model of CHO on the image domain by FBP reconstruction. The result will demonstrate the feasibility of building an observer model based on sinogram data, which would bring up the first step of developing ideal observer model for sinogram data. We believe it is meaningful because that sinogram data reveal fundamental quality property of the CT hardware and preprocessing algorithm. An ideal observer that attains the upper bound of the quality assessment performance will be used to justice not only the CT device performance, but also the performances of sinogram preprocessing and reconstruction algorithms.

Observer model focuses on object detection task in a local region, which discriminates a local signal from its background in reference to the recognizing capability of the human vision system. The main challenge of conducting model observer is that in the sinogram domain, a local image structure corresponds to a narrow sine strip and all the trips of structures superpose together to form the entire sinogram. Obviously, this property of sinogram does not match the arithmetic rule of CNNs, since CNNs specifically explores and synthesizes local structure information. In recent years, based on the success in the natural language processing field (NLP), the transformer architecture [27] has been applied in the computer vision field [28], e.g., image quality assessment [29, 30]. Transformer architecture is more applicable in the sinogram domain [31], since transformer designs a self-attentional mechanism to capture global interactions between contexts [32]. In this paper, we proposed a transformer-based model observer in sinogram domain for SKE/BKS detection tasks, where the background is known statistically due to the random background artifacts. Note that our motivation is to evaluate the influence of artifacts and noise in supervised learning, where the full-dose sinograms are known exactly. Hence, the background artifacts are obtained by subtracting the full-dose sinograms from low-dose sinograms. We implement the transformer-based model observer in these background artifacts. The proposed transformer-based model observer is then employed to assess modern supervised CNN-based sinogram domain denoising methods. Three canonical CNN-based denoising methods are identified for analysis, including RED-CNN [33], DnCNN [6, 34].

The remainder of the paper is organized as follows. Section II describes the background on binary signal detection task and presents the transformer-based model observer. Section III provides the numerical studies and the results of the proposed evaluations of different denoising networks. Section IV draws the conclusions.

## METHODS

### Laguerre-Gauss Channelized Hotelling Observer

To evaluate the detectability, we conducted the 2 alternative forced choice (2-AFC) detection task. The hypotheses for signal-absent ( $H_0$ ) and signal-present ( $H_1$ ) are given by:

$$H_0 : \mathbf{g} = \mathbf{f}_b + \mathbf{f}_n \quad (1)$$

$$H_1 : \mathbf{g} = \mathbf{f}_s + \mathbf{f}_n \quad (2)$$

where  $\mathbf{g}$  is a column vector of the given image,  $\mathbf{f}_s$  is the signal-present background,  $\mathbf{f}_b$  is a signal-absent background,  $\mathbf{f}_n$  is noise. Our goal is to assess the quality of CT images in the SKE/BKS detection task, where the background is known statistically due to the random background artifacts.

In preliminary assessments of quality for CT images, the HO provides the upper bound of detection performance in linear model observers. To avoid estimating the large size of covariance matrix in the HO, the CHO approximate the performance of the HO with efficient channels by reducing the data dimensionality. In the CHO, Image  $\mathbf{g}$  is transformed to  $\mathbf{v}$  by

$$\mathbf{v} = \mathbf{U}\mathbf{g} \quad (3)$$

where  $\mathbf{U}$  is the channel matrix. LG-CHO uses a LG function for the channel matrix and can approximate the CHO performance for a rotationally symmetric signal in a known location. The LG function is defined as follows:

$$U_j(r|a) = \frac{\sqrt{2}}{a} \exp\left(\frac{-\pi r^2}{a^2}\right) L_j\left(\frac{2\pi r^2}{a^2}\right) \quad (4)$$

with the Laguerre polynomial function:

$$L_j(x) = \sum_{i=0}^j (-1)^i \binom{j}{i} \frac{x^i}{i!} \quad (5)$$

where  $r$  is the distance of the point of interest to the center,  $j$  denotes the  $j$ th channel and  $a$  is the width of the Gaussian function. In this work, we use 5 channels with 2 mm width of the Gaussian function. Figure 3 illustrates the appearances of the 5 channels under given Gaussian widths.

The CHO template estimated from training images is computed by:

$$\mathbf{w} = \Delta\mathbf{v}^T \mathbf{K}_v^{-1} \quad (6)$$

where  $\Delta\mathbf{v}$  is the mean difference between the signal-present and signal-absent transformed images, and  $\mathbf{K}_v^{-1}$  is the image covariance matrix,  $T$  is the transpose. The CHO decision variable can be computed by

$$d = \mathbf{w}^T \mathbf{v} \quad (7)$$

In this work, The LG-CHO is applied to ROIs cropped from the reconstructed residual image around the lesion centers. The ROIs are of size 64 pixels  $\times$  64 pixels, where the lesion size was of 9 pixels diameter with circle shape. We extract 1000 signal-present and 1000 signal-absent samples to be a training set.

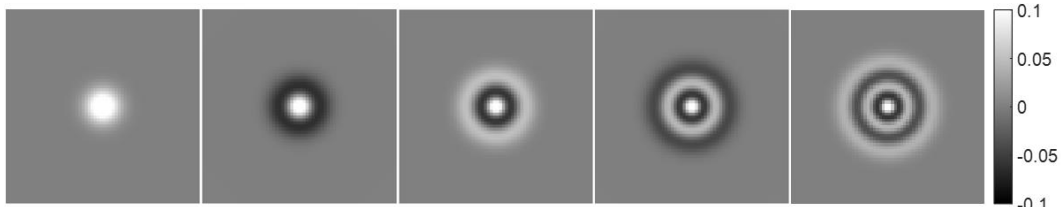


Figure 1. The appearance of the 5 LG channels of size 64 pixels  $\times$  64 pixels and Gaussian width of 10 pixels along both axes.

## Low-dose CT data preparation

We use the full-dose CT 3 mm slice from a conventional clinical dataset authorized for “the 2016 NIH-AAPM-Mayo Clinic Low Dose CT Grand Challenge” by Mayo Clinic to generate the dataset [31]. Figure 2 shows the flowchart for generating a signal-present image in liver region. we inserted a signal with circle shape near the center of the Region of Interest (ROI) by adding a CT value of 20 Hounsfield Unit (HU), to simulate a challenge task of low contrast lesion detection. After forward projection, we can obtain the full-dose signal-present sinogram, where the signal is a narrow sine strip in the sinogram domain. Poisson noise is superimposed to the sinogram to consider the statistical property. Then, we can obtain the low-dose signal-present sinogram. The filtered back projection (FBP) algorithm is employed to reconstruct the image. Table I lists the simulation parameters for fan beam CT reconstruction. The background artifacts are obtained by subtracting the full-dose signal-absent sinogram/image from low-dose signal-present sinogram/image. 64 pixels  $\times$  64 pixels ROI is extracted from the image to evaluate the LG-CHO method. 64 bins  $\times$  1160 views sine strip is extracted from the sinogram and then reshape to a matrix to generate the signal-present data for transformer-based model observer.

Table I. Simulation parameters.

Parameters	Value
Source to Iso-Center Distance	570 mm
Minimum angle	-0.456
Maximum angle	0.4526
The number of detector bins	672
The number of views	1160
Reconstructed pixel size	0.8 mm $\times$ 0.8 mm
Reconstructed matrix size	512 pixels $\times$ 512 pixels

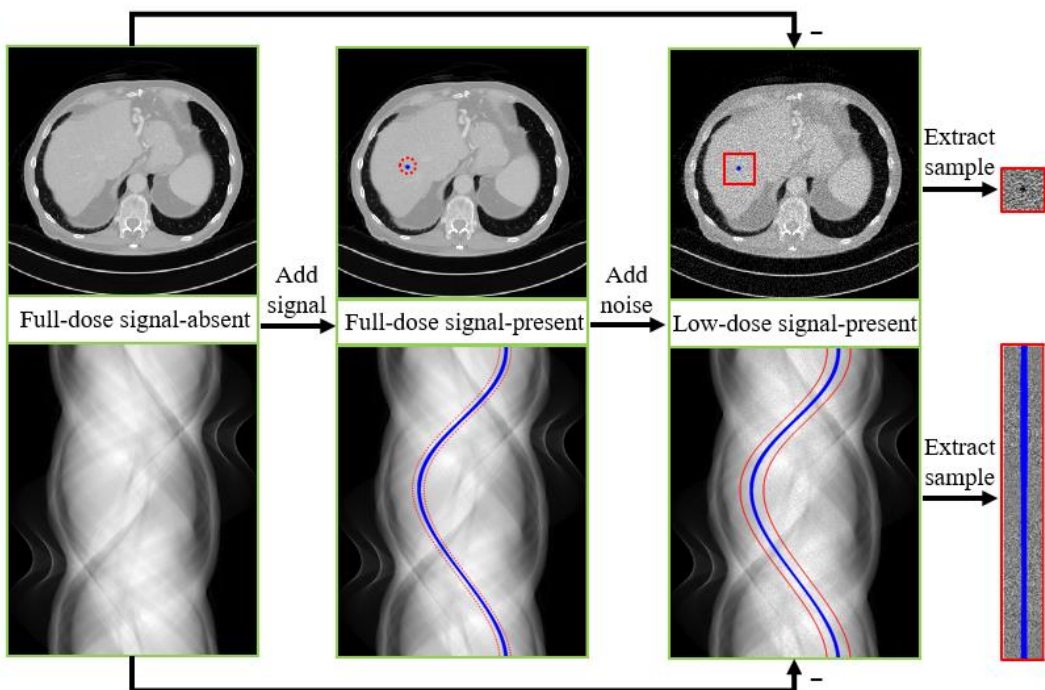


Figure 2. The flowchart of data generation.

### Transformer-based model observer

The transformer architecture can more effectively extract the sinogram feature from different view angles than CNN-based approaches because of the multi-head self-attention mechanism. In traditional vision transformer architecture, image is cut into patches as the input token of transformer to consider the spatial relation in nature images. Since each view of sinogram represents one measurement of imaging target, modeling self-attention relations between views can benefit the network to better learn the general feature under different views [26]. Thus, considering the tokenization of transformer, we split each view of the sinogram as an input token. Figure 3 shows the structure of the proposed transformer-based model observer. We modeled the detection task as a classification problem by selecting the signal-present image. For the 2-AFC detection task, the randomly selected signal-present and signal-absent sinogram pair are employed as the input of the transformer. Note that  $\dot{F}' \in \mathbb{R}^{H \times D}$  /  $F' \in \mathbb{R}^{H \times D}$  randomly represents the signal-present/signal-absent or signal-absent/signal-present sinogram pairs, where  $H$  and  $D$  are the number of detector bins and views, respectively. As often used in the vision transformer models, an extra embedding  $F_0$  is appended in the beginning of the input sinogram. we add the learnable position encodings  $P \in \mathbb{R}^{(H+1) \times D}$  to the corresponding  $F \in \mathbb{R}^{(H+1) \times D}$  to maintain the position information. The calculation of the encoder can be formulated as

$$\begin{aligned}
y_0 &= [F_0 + P_0, F_1 + P_1, \dots, F_N + P_N], \\
q_i &= k_i = v_i = y_{i-1}, \\
y'_i &= LN(MHA(q_i, k_i, v_i) + y_{i-1}), \\
y_{i-1} &= LN(MHA(y'_i) + y'_i), \quad i = 1, \dots, L \\
[E_0, E_1, \dots, E_N] &= y_L
\end{aligned} \tag{8}$$

Where  $L$  represents the number of the encoder-decoder layers. The output of the encoder  $E \in \mathbb{R}^{(H+1) \times D}$  has the same size to the input  $F$ .

The decoder takes another sinogram with extra embedding as the input. The output of the encoder,  $E$ , is used as an input of the decoder in the second MHA layer. The calculation of the decoder can be formulated as

$$\begin{aligned}
y_L &= [E_0, E_1, \dots, E_N], \\
z_0 &= [\dot{F}_0 + \dot{P}_0, \dot{F}_1 + \dot{P}_1, \dots, \dot{F}_N + \dot{P}_N], \\
q_i &= k_i = v_i = z_{i-1}, \\
z'_i &= LN(MHA(q_i, k_i, v_i) + z_{i-1}), \\
z_{i-1} &= LN(MHA(y'_i) + y'_i), \quad i = 1, \dots, L \\
[\dot{E}_0, \dot{E}_1, \dots, \dot{E}_N] &= y_L
\end{aligned} \tag{9}$$

The output  $\dot{E} \in \mathbb{R}^{(H+1) \times D}$  of the decoder is finally obtained to feed in to the following MLP head.

The MLP head consists of two fully connected (FC) layers, and the first FC layer is followed by ReLU activation. The second FC layer is followed by the Sigmoid activation to predict the labels of signal-present and signal-absent sinogram pair.

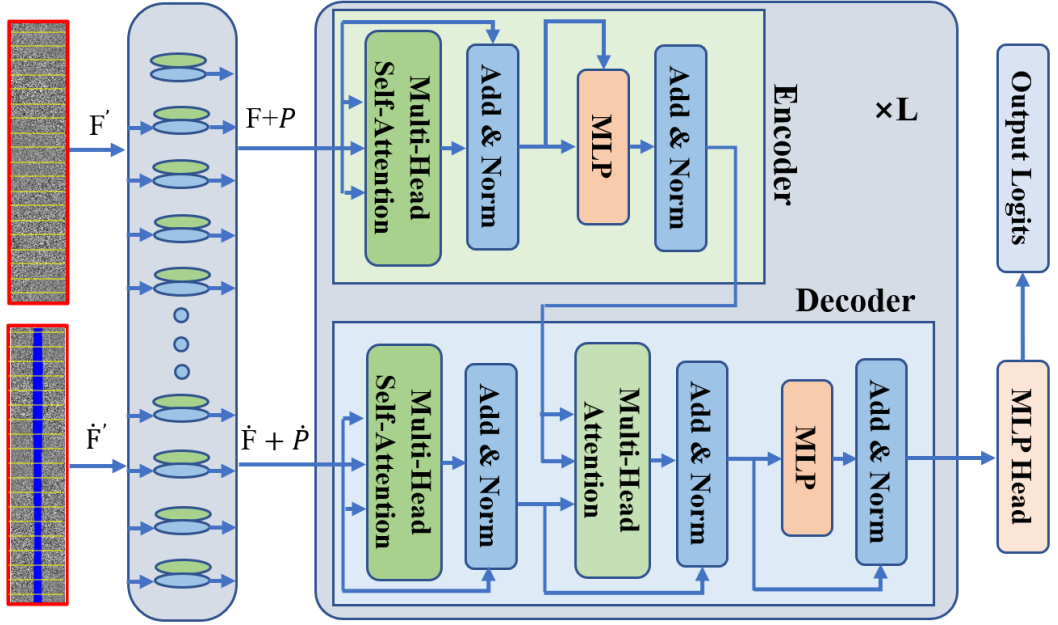


Figure 3. Model architecture of the proposed transformer-based model observer.

During network training, the hyper-parameters for the model are set as follow: The number of encoder and decoder layer is set to 1. The number of heads in the MHA is set to 4. The transformer dimension is set to 1160. The dimension of the MLP in the encoder and decoder is set to 1024. The dimension of the first FC layer in MLP head is set to 128. The dimension of the patches fed into the transformer is  $64 \times 1160$ . The training is conducted using an Adam optimizer with a batch size of 16. Initial learning rate 0.00005 and cosine learning rate decay are set. The training loss is computed using an entropy cross loss function. The number of epochs is set to 200. Our network is implemented using Pytorch framework with a single NVIDIA GeForce 3090 GPU. To train our network, we use 5000 signal-present sinograms and 5000 signal-absent sinograms since our detection task is 2-AFC. We divide the generated datasets into 0.95:0.05 ratio for training dataset and validation dataset.

### Denoising networks

To evaluate the proposed model observer in deep learning based low-dose CT algorithms, two classical networks were employed for projection domain denoising, including RED-CNN and DnCNN. A real clinical dataset authorized by Mayo Clinics for “the 2016 NIH-AAPM-Mayo Clinic Low Dose CT Grad Challenge” was used to validate the performance of the networks. In the training step, 9 patients were selected as training set. 1 patient was selected as testing set. We used the normal-dose images from the dataset to simulate the low dose sinograms. For RED-CNN, the network architecture was set the same as in [28]. For DnCNN, the network architecture was set the same as in [29]. The training is conducted using an Adam optimizer with a batch size of 16. Initial learning rate is 1e-5 for RED-CNN and 1e-3 for DnCNN. The training loss is computed using a mean-square-error (MSE) loss function. The number of epochs is set to 100.

### Evaluation of detection performance

We used percent correct ( $P_c$ ) as a detection performance measure for the model observers, which was calculated as:

$$P_c = \frac{1}{N_t} \sum_{i=1}^{N_t} o_i \quad (10)$$

where  $N_t$  is the number of test trials and  $o_i$  is binary decision variables, that is  $o_i$  can only be 1 or 0, corresponding to correct or incorrect detection results, respectively. To obtain  $o_i$ , we compared the correct answer with the logit of the network output. In case of LG-CHO, we selected the image which had the largest decision variable between 2 input images and compared it with the correct answer. We use 1000 sinogram pairs (i.e., 1000 signal absent sinograms and 1000 signal present sinograms) as test dataset to evaluate the performance of our proposed transformer-based model observer. The corresponding 1000 image pairs (i.e., 1000 signal absent images and 1000 signal present images) are used as test dataset to evaluate the performance of LG-CHO.

## RESULTS

### Detectability in different noise level.

Figure 4 shows the sinograms/images with 100, 50, 25 thousand incident photons. With the decrease of incident photons, the signal-to-noise ratio (SNR) of the sinograms/images is reduced. Some fine details are obscured by noise, which are important in clinical diagnosis, e. g., lesion detection. We use numerical observer models to evaluate the detectability by extracting ROIs in sinograms/images.

Figure 5 shows some samples in training dataset. The circular signal is inserted in the center of ROIs in the artifact images to simulate a challenge task of low contrast lesion detection. The signal in sinogram is corresponding a narrow strip. The signal is difficult to distinguish visually in both artifact images and sinograms for this challenge task, because it is affected by noise.

Figure 6 shows the performance curves of the signal detectability versus the dose level. It can be seen from the curves that the performance trends among LG-CHO and transformer-based model observer are similar. This simiar trend shows that our proposed transformer-based model observer can be used to evaluate the signal detection task in sinogram domain.

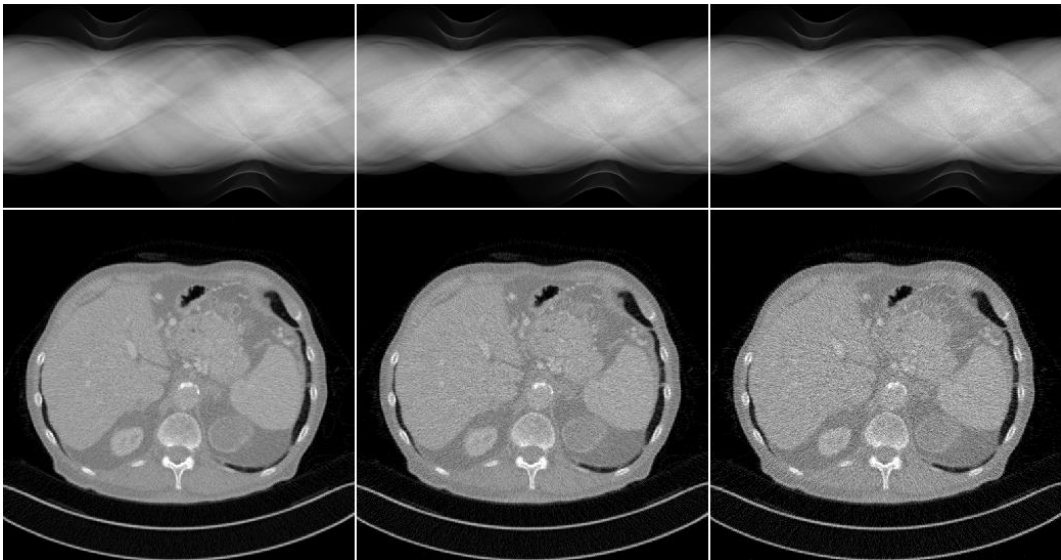


Figure 4. From left to right are the sinograms/reconstructed images with 100, 50, 25 thousand incident photons. Top is the sinograms with display window [0, 9]. Bottom is the corresponding reconstructed images with display window [0, 0.035] mm<sup>-1</sup>.

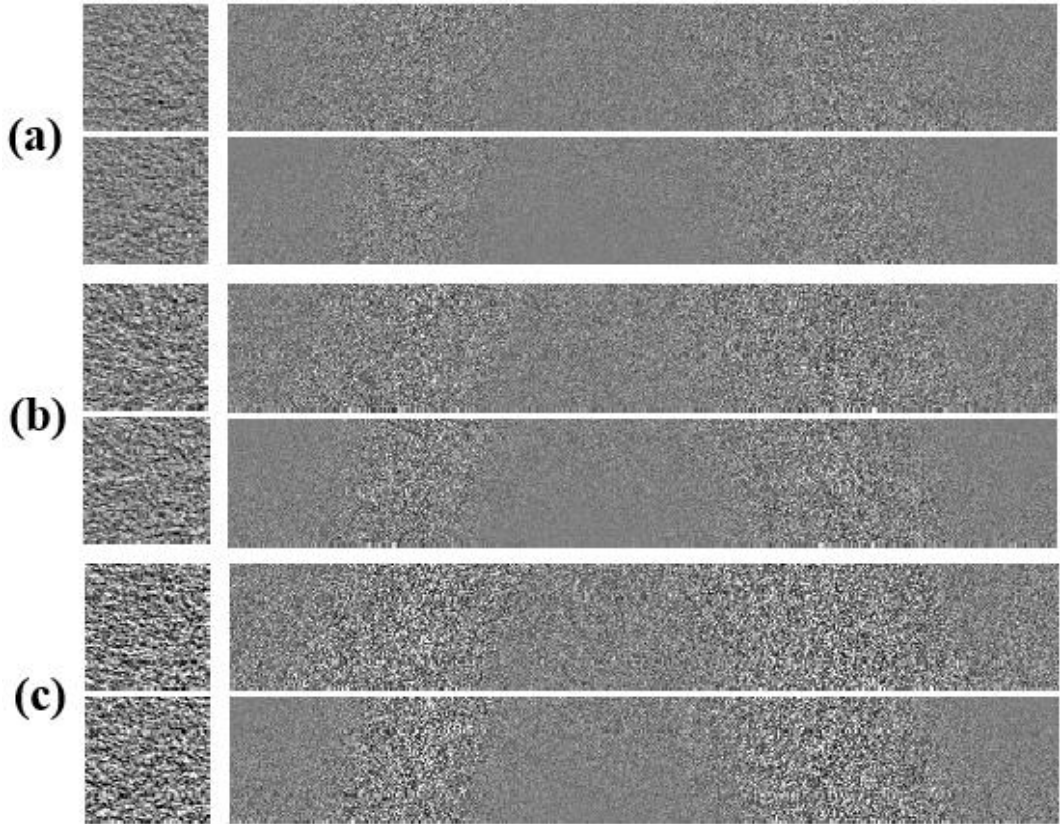


Figure 5. Some samples in training dataset. From (a)-(c) are the images/sinograms with 100, 50, 25 thousand incident photons. For each group in (a)-(c), top is the signal-present images/sinograms, bottom is the signal-absent images/sinograms. Left is the ROIs from the images with display window  $[-0.005, 0.005]$ . Right is the ROIs from the sinograms with display window  $[-0.5, 0.5]$ .

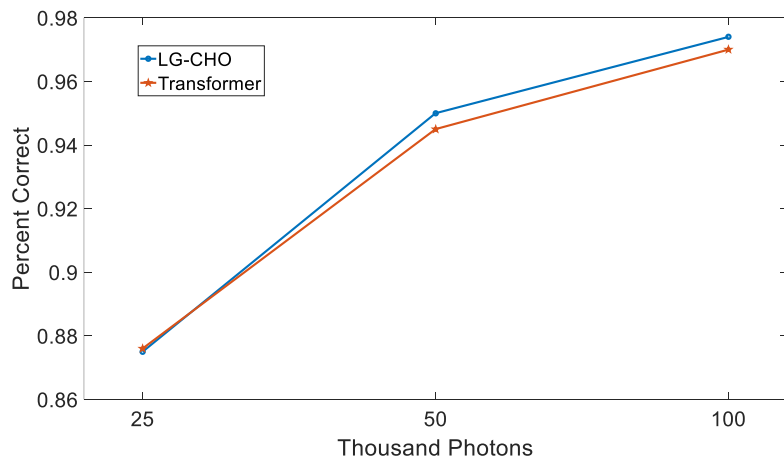


Figure 6. The lesion detectability curves associated with different dose levels.

#### Evaluation of Denoising network

Figure 7 shows the sinograms/images with 25 thousand incident photons, the results reconstructed by RED-CNN and DnCNN. The noise is suppressed after being processed by the denoising networks of RED-CNN and DnCNN. Table II shows the quantitative results from different denoising networks on the whole testing set images. It can be seen that the RED-CNN method produced the images with

the highest peak signal-to-noise ratio (PSNR), root-mean-square error (RMSE) and structure similarity index (SSIM). DnCNN also improves on these quantitative metrics. However, some fine details are blurred. For example, the dots indicated by the red arrow can be seen in the original low-dose CT image, but are blurred in the images processed by the denoising networks. This is because both RED-CNN and DnCNN employ the MES loss to train the network, which guarantees the global image optimality but not guarantee the task-specific optimality, e. g., lesion detection. Especially for DnCNN, the introduction of some secondary artifacts also degrades the image quality.

Figure 8 shows some samples in training dataset. After processed by RED-CNN and DnCNN, the noise is suppressed. However, some structures are enhanced in the residual sinograms, which causes the blurred images. Both the blur in image domain and the enhanced structure in residual projection domain influence the performance of the numerical observer models.

Figure 9 shows the performance curves of the signal detectability versus different methods. It can be seen from the curves that the performance trends among LG-CHO and transformer-based model observer are similar. And the proposed transformer-based model observer perform better than LG-CHO. However, the detectability decrease after the image prepossessed by the denoising networks, which is consistent to the visual inspection. The fine details are removed by the denoising networks, which reduce the detectability. Hence, it is desireable to propose a method that can improve the metrics of RMSE/PNSR/SSIM and LG-CHO/Transformer-based observer simultaneously, since the detectability is important in clinical diagnosis.

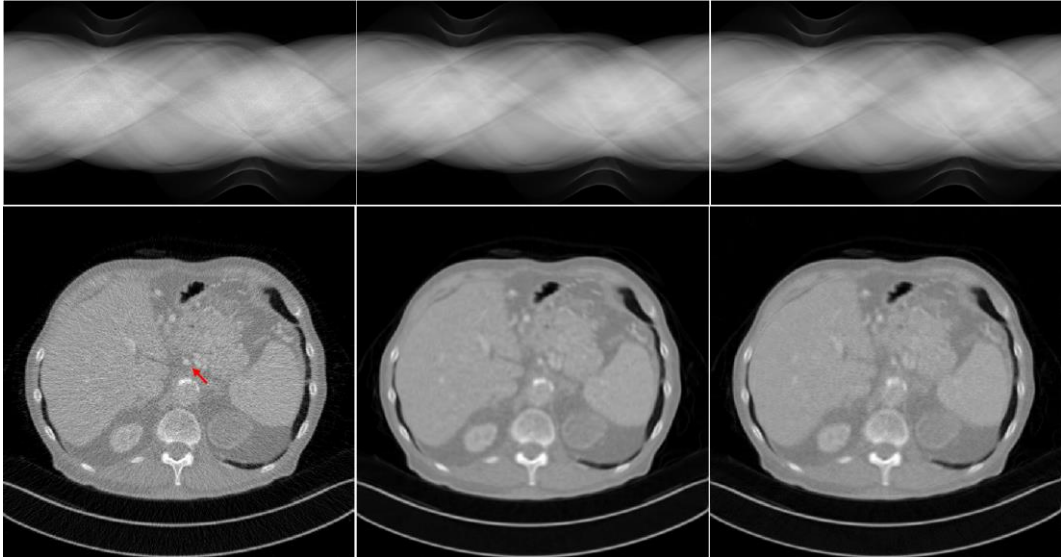


Figure 7. From left to right are the sinograms/images with 25 thousand incident photons, the results reconstructed by RED-CNN and DnCNN. Top is the sinograms with display window [0, 9]. Bottom is the corresponding reconstructed images with display window [0, 0.035] mm<sup>-1</sup>.

Table II. Quantitative results of different denoising networks.

Methods	Low dose	RED-CNN	Dn-CNN
RMSE	0.0069	0.0025	0.0038
PNSR	43.4594	52.0860	48.3616
SSIM	0.9608	0.9981	0.9879

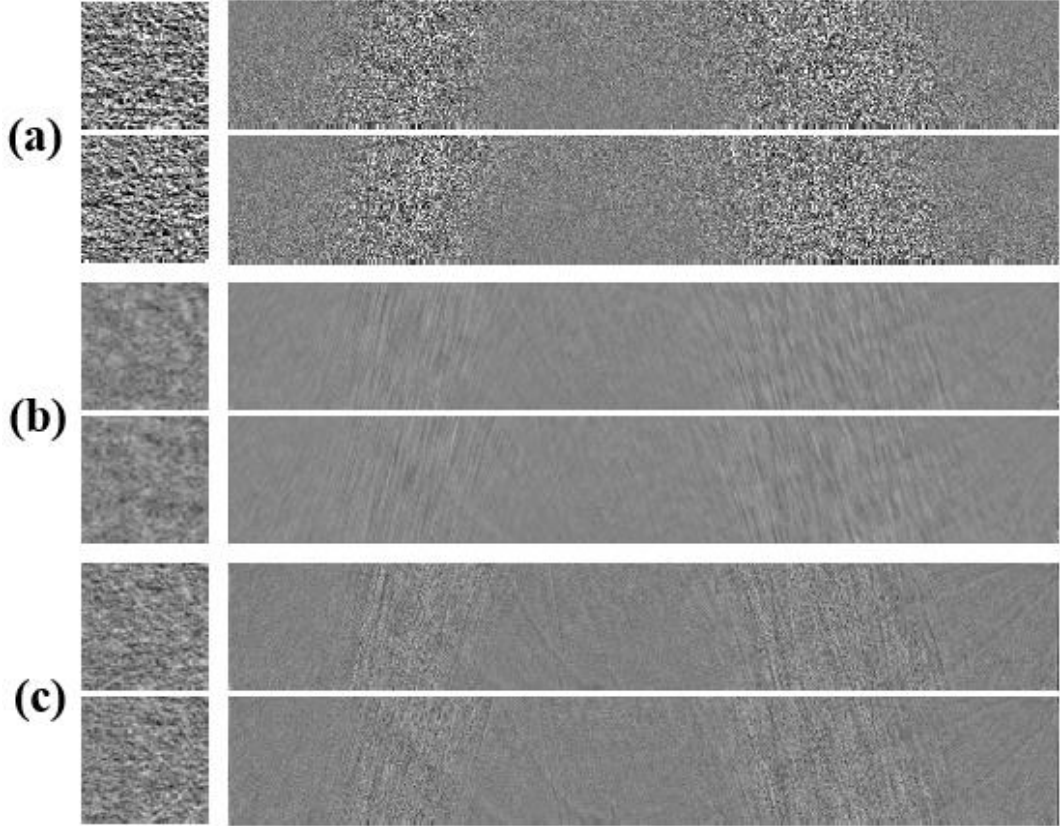


Figure 8. Some samples in training dataset. From (a)-(c) are the images/sinograms with 25 thousand incident photons, the results reconstructed by RED-CNN and DnCNN. For each group in (a)-(c), top is the signal-present images/sinograms, bottom is the signal-absent images/sinograms. Left is the ROIs from the images with display window  $[-0.005, 0.005]$ . Right is the ROIs from the sinograms with display window  $[-0.5, 0.5]$ .

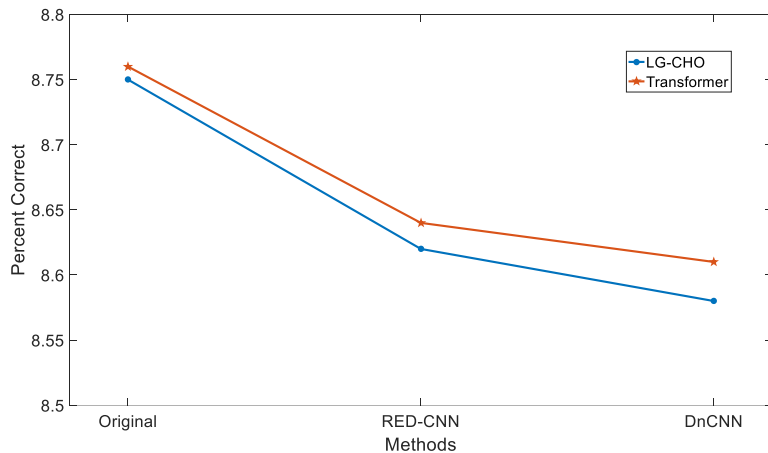


Figure 9. The lesion detectability curves associated with different dose levels.

## DISCUSSIONS AND CONCLUSION

In this work, we have demonstrated that the transformer-based model observer yields a performance similar to the LG-CHO for detection of a circular signal for an SKE/BKS with a residual background. Hence, the reference images are required to calculate the residual background. However,

in practice the reference images are usually difficult to obtain. Furthermore, the proposed transformer-based method belongs to the ideal observer, which is still not the same as the human observer. Implementing an anthropomorphic model observer using a transformer-based model is another interesting topic, which will not rely on reference images and bring the results closer to what the human observer achieves. A large amount of data labeled by a human observer should be prepared for training the transformer-based anthropomorphic model observer, which is a future topic for our research.

We have evaluated two low-dose CT sinogram domain denoising methods in this work. However, there are numerous sinogram denoising methods including both traditional methods and deep learning-based methods. In our future work, we will evaluate more denoising methods, including traditional methods. Also, the impact of the parameters of the denoising networks on task-specific performance measures will be evaluated; e. g., the depth of the networks.

In conclusion, we proposed a transformer-based model observer to evaluate the low dose CT sinogram domain supervised learning methods. With the help of transformer, the proposed transformer-based observer model showed a similar performance with conventional LG-CHO models. However, LG-CHO has strict assumption (i.e., rotationally symmetric signal, known location, and stationary background) to approximate the ideal linear observer performance. In contrast, the transformer-based observer model can be less restrictive from those conditions. In addition, the evaluation in sinogram domain can avoid the image reconstruction, which may suggest future avenues for improving the effectiveness of sinogram domain supervised learning methods. That is to improve the metrics of RMSE/PNSR/SSIM and LG-CHO/Transformer-based observer simultaneously. In general, the further work is to build an ideal observer model based on sinogram data that achieves the upper bound of the evaluation performance of a sinogram data, which would be used to guide the optimizations of CT scanner developments and sinogram preprocessing and reconstruction algorithms.

## REFERENCES

- [1] T. Li, X. Li, J. Wang et al., “Nonlinear sinogram smoothing for low-dose X-ray CT,” *IEEE Transactions on Nuclear Science*, vol. 51, no. 5, pp. 2505–2513, 2004.
- [2] J. Wang, T. Li, H. Lu et al., “Penalized weighted least-squares approach to sinogram noise reduction and image reconstruction for low-dose X-ray computed tomography,” *IEEE Transactions on Medical Imaging*, vol. 25, no. 10, pp. 1272–1283, 2006.
- [3] A. Manduca, L.F. Yu, J.D. Trzasko et al., “Projection space denoising with bilateral filtering and CT noise modeling for dose reduction in CT,” *Medical Physics*, vol. 36, no. 11, pp. 4911–4919, 2009.
- [4] M. Balda, J. Hornegger, B. Heismann, “Ray contribution masks for structure adaptive sinogram filtering,” *IEEE Transactions on Medical Imaging*, vol. 31, no. 6, pp. 1228–1239, 2012.
- [5] H. Zhang, L. Zhang, Y. Sun, J. Zhang, “Projection domain denoising method based on dictionary learning for low-dose CT image reconstruction,” *Journal of X-ray Science and Technology*, vol. 23, no. 5, pp. 567-78, 2015.
- [6] M. U. Ghani, W. C. Karl, “CNN based sinogram denoising for low-dose CT,” *Mathematics in Imaging*, 2018.

- [7] M. Meng, S. Li, L. Yao et al., “Semi-supervised learned sinogram restoration network for low-dose CT image reconstruction,” *SPIE Medical Imaging*, p. 11312, 2020.
- [8] Y. J. Ma, Y. Ren, P. Feng et al., “Sinogram denoising via attention residual dense convolutional neural network for low-dose computed tomography,” *Nuclear Science and Techniques*, vol. 32, no. 4, pp. 1-14, 2021.
- [9] L. Chao, P. Zhang, Y. Wang et al., “Dual-domain attention-guided convolutional neural network for low-dose cone-beam computed tomography reconstruction,” *Knowledge-Based Systems*, p. 109295, 2022.
- [10] Z. Wang, A. C. Bovik, H. R. Sheikh et al., “Image quality assessment: from error visibility to structural similarity,” *IEEE transactions on image processing*, vol. 13, no. 4, pp. 600-612, 2004.
- [11] L. Zhang, L. Zhang, X. Mou et al., “FSIM: A feature similarity index for image quality assessment,” *IEEE transactions on Image Processing*, vol. 20, no. 8, pp. 2378-2386, 2011.
- [12] S. Richard, D. B. Husarik, G. Yadava et al., “Towards task - based assessment of CT performance: system and object MTF across different reconstruction algorithms,” *Medical Physics*, vol. 39, no. 1, pp. 4115-4122, 2012.
- [13] S. N. Friedman, G. S. Fung, J. H. Siewerssen et al., “A simple approach to measure computed tomography (CT) modulation transfer function (MTF) and noise - power spectrum (NPS) using the American College of Radiology (ACR) accreditation phantom,” *Medical Physics*, vol. 40, no. 5, p. 051907, 2013.
- [14] H. H. Barrett, K. J. Myers, “Foundations of image science,” *John Wiley & Sons*, 2013.
- [15] H. H. Barrett, K. J. Myers, B. D. Gallas et al., “Megalopinakophobia: its symptoms and cures,” *SPIE Medical Imaging*, pp. 299-307, 2001.
- [16] B. D. Gallas, H. H. Barrett, “Validating the use of channels to estimate the ideal linear observer,” *JOSA A*, vol. 20, no. 9, pp. 1725-1738, 2003.
- [17] X. He, S. Park, “Model observers in medical imaging research,” *Theranostics*, vol. 3, no. 10, p. 774, 2013.
- [18] R. Zeng, S. Park, P. Bakic et al., “Evaluating the sensitivity of the optimization of acquisition geometry to the choice of reconstruction algorithm in digital breast tomosynthesis through a simulation study” *Physics in Medicine & Biology*, vol. 60, no. 3, p. 1259, 2015.
- [19] S. Park, J. M. Witten, K. J. Myers, “Singular vectors of a linear imaging system as efficient channels for the Bayesian ideal observer,” *IEEE transactions on medical imaging*, vol. 28, no. 5, pp. 657-668, 2008.
- [20] J. M. Witten, S. Park, K. J. Myers, “Partial least squares: a method to estimate efficient channels for the ideal observers,” *IEEE Transactions on medical imaging*, vol. 29, no. 4, pp. 1050-1058, 2010.
- [21] D. Gomez-Cardona, C. P. Favazza, S. Leng et al., “Task-specific efficient channel selection and bias management for Gabor function channelized Hotelling observer model for the assessment of x-ray angiography system performance,” *Medical physics*, vol. 48, no. 7, pp. 3638-3653, 2021.
- [22] F. K. Kopp, M. Catalano, D. Pfeiffer et al., “CNN as model observer in a liver lesion detection task for x-ray computed tomography: A phantom study,” *Medical physics*, vol. 45, no. 10, pp. 4439-4447, 2018.

- [23] G. Kim, M. Han, H. Shim et al., “A convolutional neural network - based model observer for breast CT images,” *Medical physics*, vol. 47, no. 4, pp. 1619-1632, 2020.
- [24] H. Gong, J. G. Fletcher, J. P. Heiken et al., “Deep-learning model observer for a low-contrast hepatic metastases localization task in computed tomography,” *Medical physics*, vol. 49, no. 1, pp. 70-83, 2022.
- [25] K. Li, W. Zhou, H. Li et al., “Assessing the impact of deep neural network-based image denoising on binary signal detection tasks,” *IEEE transactions on medical imaging*, vol. 40, no. 9, pp. 2295-2305, 2021.
- [26] Q. De Man, E. Haneda, B. Claus et al., “A two-dimensional feasibility study of deep learning-based feature detection and characterization directly from CT sinograms,” *Medical physics*, vol. 46, no. 12, pp. e790-e800, 2019.
- [27] A. Vaswani, N. Shazeer, N. Parmar et al., “Attention is all you need,” *Advances in neural information processing systems(NIPS)*, 2017.
- [28] A. Dosovitskiy, L. Beyer, A. Kolesnikov et al., “An image is worth 16x16 words: Transformers for image recognition at scale,” arXiv preprint arXiv:2010.11929, 2020.
- [29] J. You, J. Korhonen, “Transformer for image quality assessment,” *IEEE International Conference on Image Processing (ICIP)*, pp. 1389-1393, 2021.
- [30] M. Cheon, S. J. Yoon, B. Kang et al., “Perceptual image quality assessment with transformers,” *Proceedings of the IEEE/CVF Conference on Computer Vision and Pattern Recognition*, pp. 433-442, 2021.
- [31] L. Yang, Z. Li, R. Ge et al., “Low-Dose CT Denoising via Sinogram Inner-Structure Transformer,”. *IEEE Transactions on Medical Imaging*, Early Access, 2022.
- [32] J. Liang, J. Cao, G. Sun et al., “Swinir: Image restoration using swin transformer,” *Proceedings of the IEEE/CVF International Conference on Computer Vision*, pp. 1833-1844, 2021.
- [33] H. Chen, Y. Zhang, M. K. Kalra et al., “Low-dose CT with a residual encoder-decoder convolutional neural network,” *IEEE transactions on medical imaging*, vol. 36, no. 12, pp. 2524-2535, 2017.
- [34] K. Zhang, W. Zuo, Y. Chen et al., “Beyond a gaussian denoiser: Residual learning of deep CNN for image denoising,” *IEEE transactions on image processing*, vol. 26, no. 7, pp. 3142-3155, 2017.